Estuaries and Coasts
https://doi.org/10.1007/s12237-020-00784-3

Sediment Budget Estimates for a Highly Impacted Embayment with Extensive Wetland Loss

Robert J. Chant[1] · David K. Ralston[2] · Neil K Ganju[3] · Cassia Pianca[4] · Amy E. Simonson[5] · Richard A. Cartwright[5]

Received: 21 December 2018 / Revised: 22 May 2020 / Accepted: 12 June 2020

Abstract

External sediment supply is an important control on wetland morphology and vulnerability to storms, sea-level rise, and land use change. Constraining sediment supply and net budgets is difficult due to multiple timescales of variability in hydrodynamic forcing and suspended sediment concentrations, as well as the fundamental limitations of measurement and modeling technologies. We used two independent observational campaigns and one hydrodynamic modeling effort to estimate the sediment supply to Jamaica Bay, New York, USA, an urbanized embayment with a history of extensive wetland loss. We found that all three estimates indicate a net import to the system, ranging from 36 to 74 kt/year, with a mean estimate of 55 kt/year ± 31 kt/year, which is consistent with a prior estimate derived from radionuclide tracers. Net sediment import is controlled by flood-ebb asymmetry in bed shear stress, which results in higher suspended sediment concentrations on flood tide relative to ebb. This indicates a seaward source of sediment that is resuspended by waves in the coastal ocean, likely offshore marine deposits or potentially from the adjacent Hudson River estuary. Despite the net sediment import, a simple sediment budget suggests that the rate of supply is not sufficient to maintain the present geomorphic planform of the system relative to sea-level rise. The convergent estimates from independent methods provide reasonable guidance as context for sediment-based restoration efforts.

Keywords Sediment transport · Wetland loss · Estuarine dynamics · Human impacted coastal · Systems

Introduction

Salt marshes are ephemeral coastal features modulated by hydrodynamic forcing, sediment transport, and biological feedbacks [Fagherazzi et al. 2013a; Friedrichs and Perry 2001]. Rarely in equilibrium, they contract or expand in response to sea level [Kirwan and Megonigal 2013], wave attack, and variability in sediment supply [Mariotti and Fagherazzi 2013]. Other factors, such as herbivory [Holdredge et al. 2009] and eutrophication [Deegan et al. 2012], can contribute to instability, which may lead to contraction through loss of the vegetated plain. In many estuaries and coastal embayments, increasing rates of salt marsh loss due to sea-level rise, wave-induced erosion, and sediment deficits have spurred efforts to quantify marsh vulnerability and lifespan.

Salt marshes provide critical ecosystem services including carbon sequestration, habitat provision, and wave attenuation [Barbier et al. 2011]. These services are largely a function of marsh areal coverage and elevation in the local tidal range, both of which are partially controlled by external sediment supply. In the absence of sea-level rise, regular wave-induced erosion competes with sediment supply to control the geomorphic planform of an entire marsh complex (i.e., channels, intertidal flats, scarps, and marsh plains). However, marshes are rarely in equilibrium because erosion and sediment supply are typically uncoupled, and either erosion dominates and marshes retreat or sediment supply dominates and marshes expand [Donatelli et al. 2018; Fagherazzi et al. 2013a; Fagherazzi et al. 2013b, Leonardi et al. 2016]. Sea-level rise imposes additional requirements on the sediment supply to maintain equilibrium by creating accommodation space that must be filled for the marsh to maintain a constant

Communicated by Paul A. Montagna

✉ Robert J. Chant
chant@marine.rutgers.edu

[1] Department of Marine and Coastal Sciences, Rutgers University, New Brunswick, NJ, USA

[2] Woods Hole Oceanographic Institution, Woods Hole, MA, USA

[3] Woods Hole Coastal and Marine Science Center, U.S. Geological Survey, Woods Hole, MA, USA

[4] Virginia Institute of Marine Sciences, William and Mary, Gloucester Point, VA, USA

[5] New York Water Science Center, U.S. Geological Survey, Buffalo, NY, USA

Published online: 01 July 2020

elevation with respect to sea level. Marsh trajectory can be inferred through sediment transport metrics within tidal channels, which spatiotemporally integrate factors contributing to sediment supply and consequently marsh contraction and expansion [Ganju et al. 2013].

External sediment supply to marshes can arise from river input [Reed 2002], resuspension of fine sediment from the estuarine and marine seabed [Goodbred and Hine 1995], resuspension by waves [Fagherazzi and Priestas 2010], and/or erosion of coastal headlands. Land practices, including damming and urbanization, have reduced natural sediment loads to some estuaries [Weston 2014]. Previous land use practices like clearance for agriculture and hydraulic mining increased sediment supply relative to the natural background and may have contributed to the creation of many present-day marsh complexes [Barnard et al. 2013; Ganju et al. 2013]. Other anthropogenic sources include the use of dredged material, which can be deposited on vulnerable marsh surfaces to increase elevation relative to the tidal frame [Ford et al. 1999].

One prominent example of a marsh complex that has experienced significant loss is Jamaica Bay (NY, USA). Based on the historical evidence for the geomorphic change of Jamaica Bay over several centuries, Sanderson (2016) postulated that the current embayed, vegetated configuration of the bay interior developed in the past few hundred years due to westward elongation of the Rockaway Peninsula, which is the southern seaward boundary of Jamaica Bay (Fig. 1). The peninsula, once fully elongated, protected the embayment from exposure to erosive waves from the Atlantic Ocean and allowed for rapid deposition of marine and watershed-derived sediment. However, while late eighteenth century maps depict the bay with vegetated shorelines but limited marsh islands [Sanderson 2016], recent cores from two of the bays island marshes suggest that the marshes extended back from well before the seventeenth century [Peteet et al. 2018]. In recent decades, however, there is a well-documented loss of marsh area in a time period that coincided with significant anthropogenic pressures including hardening of the shoreline, dredging of navigational channels, and discharge of municipal sewage into the bay. Currently, sea-level rise in this region is 3–4 mm/year [Kopp 2013], which threatens marsh sustainability if sediment supply is insufficient. Sediment budgets have not been well constrained in Jamaica Bay, and given on-going loss of marsh and expected acceleration of sea-level rise, there is a clear need for detailed investigation of the bay's sediment budget to help gauge its future geomorphic trajectory.

This paper presents data from fixed instrumentation, shipboard surveys, and numerical modeling to assess the direction and magnitude of net sediment transport between Jamaica Bay and the coastal ocean, as well as the mechanisms that drive the net sediment transport associated with tides, winds, and waves. We place these estimates of sediment transport in context with local rates of sea-level rise to determine whether the sediment supply to Jamaica Bay is sufficient to maintain vertical accretion across the estuarine and marsh complex. The topic of marsh sediment supply and the methodology employed here to assess it has broad applicability in coastal regions threatened by increasing rates of sea-level rise, particularly those that are also impacted by local anthropogenic pressures.

Study Site

Jamaica Bay is located in Brooklyn and Queens, New York City, USA, on the western end of Long Island (Fig. 1). The bay is connected to the Atlantic Ocean through Rockaway Inlet. Numerous dredging projects commenced in the bay in the late nineteenth century [Black 1981]. The inlet was stabilized by a jetty in 1934 and channel depth at the mouth is maintained for navigation at ~40 ft. (12 m). Channels in the interior of the bay were deepened to 10 m in the 1930s to provide navigational access to the interior of the bay, and sand mining has deepened the eastern reaches of the bay, most notably Grassy Bay. This deepening resulted in the loss of several marsh islands [Black 1981]. In recent decades, dredging has been confined to the very western end of Rockaway Peninsula. Major shoreline hardening projects include the construction of John F. Kennedy Airport in 1943 (originally Idlewild Airport) on the eastern shore and the construction of the Belt Parkway along the northern boundary of the bay, and the vast majority of the shoreline has been hardened by bulkheading and riprap. The watershed for Jamaica Bay includes the densely populated boroughs of Brooklyn and Queens of New York City, and the dominant source of freshwater to the bay today is from municipal sewage discharge from 4 major treatment plants with a total flow rate of 10 m^3/s that contains 92% of the 15,800 kg/day of total nitrogen discharged into the bay [Benotti et al. 2007]. Tides in the bay are largely semidiurnal with a range of approximately 2 m (Fig. 2a) and have increased over the past century by up to 40% due to the channel deepening [Swanson and Wilson 2008].

Over the past century, the wetlands of Jamaica Bay have significantly deteriorated from a coverage of 65 km^2 in 1907, 16 km^2 in 1970 [Hartig et al. 2002] to 3.5 km^2 in 2009 [Renfro et al. 2010]. Several processes have been cited as a possible cause for the loss of wetlands, including excess nutrients [Deegan et al. 2012], elevated wave activity associated with ship wakes [Zaggia et al. 2017], and an insufficient sediment supply relative to sea-level rise [Ganju et al. 2017]. The development and increase in impervious surface in the watershed along with the hardening of the shoreline may have reduced the local sediment supply from the watershed and erosion of the shore. Stabilization and dredging of Rockaway Inlet may have altered the supply of sediment from offshore

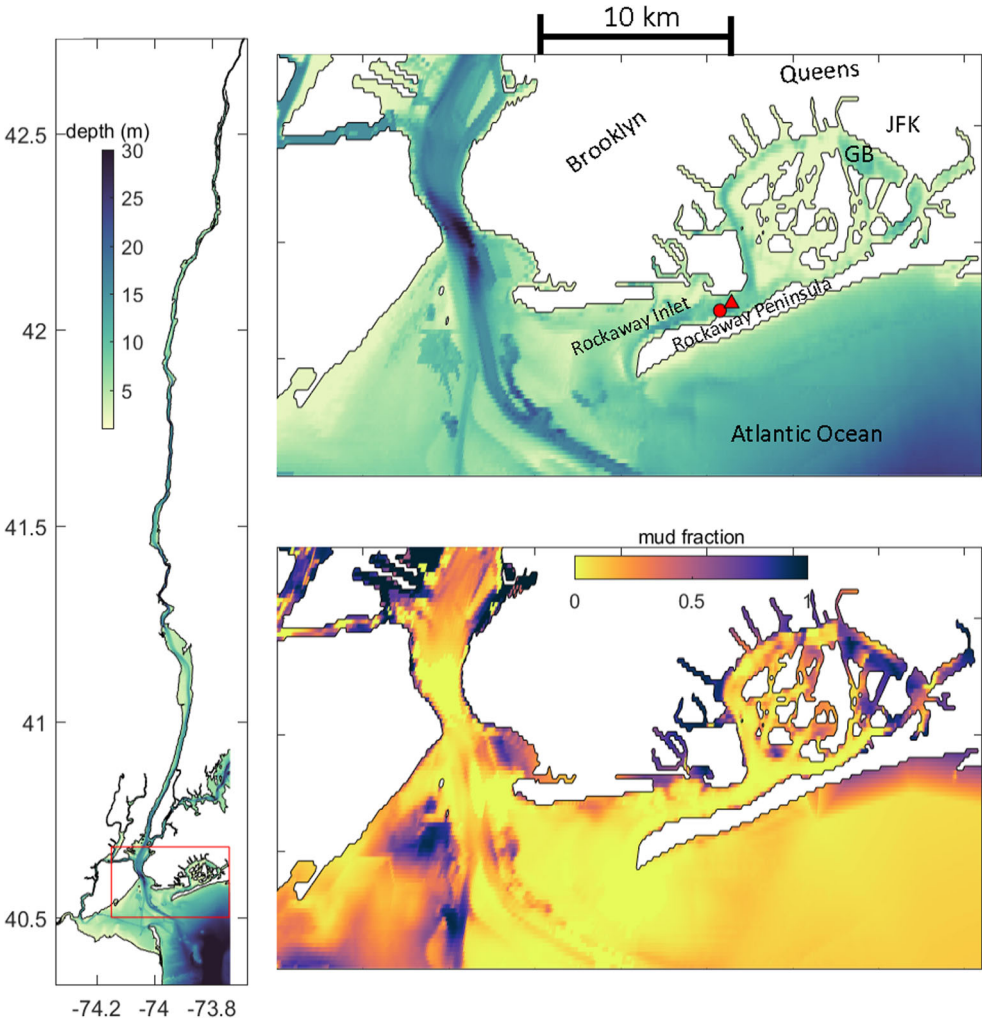

Fig. 1 Study area. (Left) Map of full model domain, (top right) zoom on JB with locations of Rutgers AWAC and ADV (red circle) and USGS side-looking ADCP, obs, and YSI (red triangle) noted. (Bottom right) Zoom on distribution of bed sediment (% mud). The USGS instrumentation is fixed to the Gil Hodges Bridge. Green regions inside Jamaica Bay (top right) are the dredged channels. JFK is John F. Kennedy Airport, and GB is Grassey Bay

and created a local sediment sink. Indeed, a sediment budget of Jamaica Bay based on radionuclide data found that signatures characteristic of marine sediment sources were predominant in the depositional record [Renfro et al. 2010]. However, that study came to significantly different estimates of the magnitude of sediment supply with two different approaches using ^{210}Pb and ^{234}Th, with the former estimate five times lower than the latter. This paper makes a direct estimate of the marine sediment supply to the bay using a combination of field and modeling studies. Together, these studies refine estimates of sediment supply to the bay, characterize the processes affecting temporal variability in the supply, and can help guide sediment-based restoration practices.

Methods

A combination of observational and modeling approaches was used to characterize sediment fluxes into Jamaica Bay. Observationally, estimates were made in Rockaway Inlet using shipboard surveys and time series from moored instruments both on the seafloor and mounted on the Gil Hodges Bridge. The approaches provide multiple means of estimating sediment fluxes as well as information on the uncertainty that would be difficult to assess with a single methodology.

In addition to the observations, a regional circulation and sediment transport model of Jamaica Bay, the Hudson River, and the coastal ocean was implemented for a period overlapping the observations. The model includes greater spatial context for the focused observations at the study site and allows evaluation of a wider range of forcing conditions. Details on the measurement and modeling approaches are provided below.

Measurements

Bottom Moorings

A mooring was maintained between 21 May 2015 and 25 August 2016 in Rockaway Inlet 500 m west of the Gil Hodges Bridge (Fig. 1). The mooring was placed in the thalweg in approximately 15 m of water on the south side of the channel. The bottom frame contained an acoustic Doppler

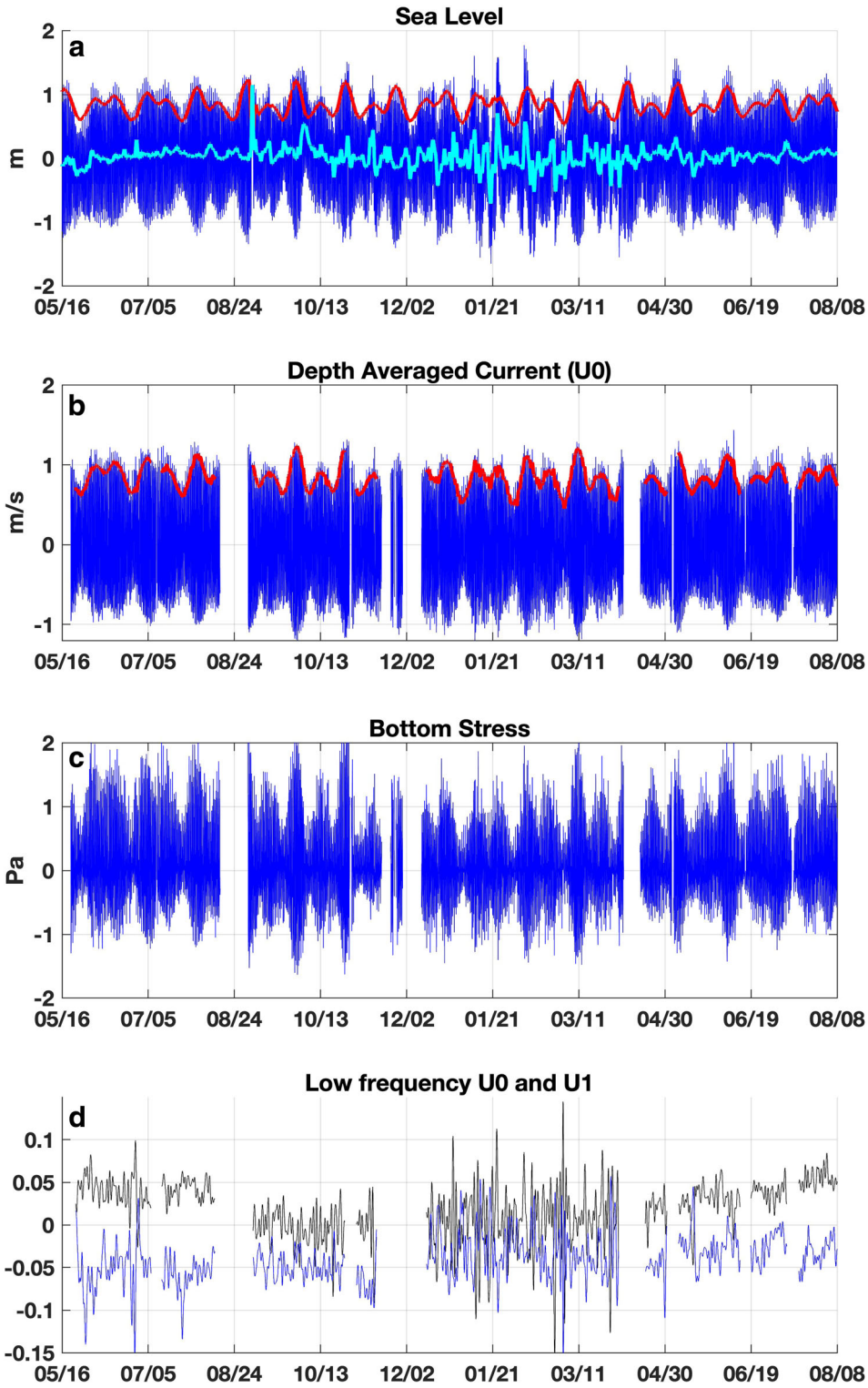

Fig. 2 **a** Sea-level at mooring location (dark blue), low passed sea-level (cyan), tidal amplitude (2b-red). **b** Depth-averaged currents (blue) and tidal current amplitude (red). **c** Bottom stress based on quadratic drag law. **d** Low passed depth-averaged current (black) and low passed shear (surface minus bottom (blue))

current profiler (1000 kHz Nortek AWAC) and surface and bottom conductivity and temperature (CT) sensors (RBR). Due to heavy fouling of the CT sensors, salinity data are limited. The AWAC collected current speeds through the water column in 0.5 m bins every 30 min. The AWAC also contained a pressure sensor from which sea-level was estimated. Surface and bottom water samples were obtained every 30 min over a spring tide tidal cycle survey and processed for suspended sediment concentration (SSC), from which calibration curves were developed to estimate SSC from the acoustic backscatter (which includes correction for beam spreading and attenuation due to both water and

sediment [Boldt 2015; Wright et al. 2010]. The vertical structure of velocity and SSC were transformed into a surface-following sigma coordinate system with 50 bins in the vertical. Time series of velocity and SSC were then filtered with a 32-h low-pass filter to isolate tidal variations (u2, tss2) from subtidal variability. The subtidal variability was further decomposed into a depth-averaged (u0, tss0) and a depth-varying component (u1, tss1). Mathematically, these are defined as

$$u0(t) = \int_{s1}^{s2}[u(s,t)]ds \quad (1)$$

$$u1(s,t) = [u(s,t)] - u0(t) \quad (2)$$

$$u2(s,t) = u(s,t) - u1(s,t) - u0(t) \quad (3)$$

with the [ ] indicating low passed velocity and s the sigma coordinate which spans from $s1$ to $s2$ covering the range of each ADCP profile. Variables $tss0$, $tss1$, and $tss2$ are defined similarly. Note that by removing the mean depth-averaged quantities ($u0$, $tss0$), both the tidal and sheared quantities ($u1$, $u2$, $tss1$, $tss2$) can be negative. We also define the low-frequency shear, Δu, as the difference between surface and bottom values of $u1$.

Combining these velocity and suspended sediment terms, we decompose sediment flux to into two terms associated with tidal and subtidal flows [Chant et al. 2011; McSweeney et al. 2016; Ralston et al. 2012a]. The first is the estuarine shear flux (F_1) and is due to the vertically varying subtidal flows ($u1$) acting on the vertically varying subtidal suspended sediment concentrations ($tss1$). The second is the tidal pumping flux (F_2), due to the covariance of tidal fluctuations in velocity ($u2$) and tidal fluctuations in suspended sediment concentration ($tss2$). Estuarine shear (F_1) and tidal pumping (F_2) sediment fluxes estimates are then:

$$F_1(t) = \int_{s1}^{s2} u1(s,t) \times tss1(s,t)ds \quad (4)$$

$$F_2(t) = \left[\int_{s1}^{s2} u2(s,t) \times tss2(s,t)ds\right] \quad (5)$$

Note that these calculations are measured in flux per unit width of the channel, and only integrate over the depths where ADCP data are available. While we could extrapolate velocity and TSS to surface and bottom, this would only have a minor impact on our assessment of the relative importance of tidal fluxes to estuarine shear fluxes. We do not calculate the mean barotropic term ($F_0 = u0 \times tss0$) here because, as discussed later, unresolved lateral shear in the channel makes this difficult to estimate with a single mooring. In the discussion, we use the freshwater discharge to the system to help constrain an estimate of this term.

In addition, we deployed an acoustic Doppler velocimeter (ADV; Sontek) for a single short-term deployment (July 8–29, 2015) in the vicinity of the AWAC mooring. The ADV measured velocity 1.2 m above the bed at 25 Hz in 5 min bursts every 30 min, and the data were used to calculate near-bed stress using the direct covariance method [Kim et al. 2000]. The acoustic backscatter from the ADV was calibrated based on estimates of SSC from the nearby AWAC.

Shipboard Surveys

A tidal cycle survey was performed during a perigean spring tides on May 5, 2016, across Rockaway Inlet in the vicinity of the mooring. The survey used a downward-looking 1200 kHz ADCP affixed to the side of the vessel and a tow-yo package consisting of a conductivity-temperature-depth sensor (CTD, RBR) and an optical backscatter sensor (OBS, D&A). Every 30 min, we completed a cycle of a northbound transect with the tow-yo package and ADCP and a southbound transect only collecting ADCP data. Following each pair of transects, water samples were obtained over the mooring and used to calibrate both the moored AWAC and the OBS. The cross-section was approximately 750 m wide and we typically obtained 20 downcasts each crossing yielding a horizontal resolution of 20–40 m. Over the ~ 12.4-h tidal cycle, 24 sections were obtained, and for each of these crossings, the sediment flux through Rockaway inlet was calculated. The sediment fluxes calculated from the cross-section surveys were used to convert the longer time series of sediment transport based on the moored instruments (kg s^{-1} m^{-1}) into net fluxes through the cross-section (kg s^{-1}). The shipboard survey was also gridded to 50-m resolution in the cross-channel direction and transformed into an s-coordinate in the vertical. Harmonic analysis was applied to the resultant time series to isolate semidiurnal (tidal) variability from lower frequency motion.

Bridge-Based Measurements

Instantaneous horizontal velocity profiles and point turbidity were measured at 6-min intervals in Rockaway Inlet under the Gil Hodges Bridge. A bridge station (USGS 01311875) fixed to the northern pier bordering the main channel consisted of a side-looking ADCP (Sontek SL500, profiling distance of 30 m, 180-s averaging interval), and a multi-parameter sonde measuring turbidity (YSI 6600). The index velocity method [Ruhl and Simpson 2005] was used to convert a reference velocity from the side-looking ADCP to the cross-sectionally averaged velocity (U_{ca}) measured via vessel transects with a downward-looking ADCP (separately from aforementioned cross-sectional surveys). Cross-sectional, velocity-weighted, depth-integrated water samples (equal depth increment method, or EDI, Edwards et al. 1999) were collected over tidal flow conditions to relate the point turbidity measured at the bridge to the SSC throughout the channel (C_{EDI}). The area of the channel (A) was calculated using the cross-section geometry and a stage-area relationship. The

instantaneous flux was then calculated as $F = U_{ca}\ C_{EDI}$ A. Extensive details are provided by Cartwright and Simonson (2019).

Modeling

Simulations using the Coupled Ocean-Atmosphere-Wave-Sediment Transport Modeling System (COAWST) [Warner et al. 2010] were evaluated to characterize sediment transport in and around Jamaica Bay. COASWT couples the Regional Ocean Modeling System (ROMS) [Haidvogel et al. 2008; Shchepetkin and McWilliams 2005], the Community Sediment Transport Modeling System (CSTMS) (Warner et al. 2008), and the SWAN wave model [Booij et al. 1999]. As described below, the wave module was activated for only a subset of the model cases. The model simulations that are analyzed here were previously developed and calibrated for other studies of the Hudson River region [Ralston and Geyer 2017; Ralston et al. 2012b; Ralston et al. 2013], and additional details on the model setup and skill assessment can be found there. The model parameters were not changed for this application to Jamaica Bay, and the model was not calibrated to the observations presented in this study.

The model domain extended from New York Bight to the tidal limit of the Hudson with a grid that was 1135 cells by 532 cells and had 16 evenly distributed sigma layers vertically. Horizontal grid resolution in the vicinity of Jamaica Bay was approximately 100 m. Open boundaries in New York Bight and Long Island Sound were forced with tidal constituents plus the observed low-pass-filtered water level from NOAA stations at Sandy Hook, NJ, and Kings Point, NY. River discharge was input for the Upper Hudson and Mohawk at the tidal limit as well as for 10 other smaller tributaries in the domain, but no freshwater discharges were prescribed into Jamaica Bay.

Sediment was represented in five independent sediment classes. Three sediment types were initially on the bed (medium sand, $w_s = 40$ mm s^{-1}; fine sand, 5 mm s^{-1}; and medium silt, 0.6 mm s^{-1}) and two additional input with river discharge (fine silt, 0.2 mm s^{-1} and very fine silt, 0.01 mm s^{-1}). Sediment properties are summarized in Table 1. Bed sediment distributions were initialized with observations [Nitsche et al. 2007] and then allowed to evolve over a 2-month spin-up period with moderate discharge and realistic tides. The model was then re-initialized with the bed sediment class distribution from the end of the spin-up with a uniform bed thickness of 0.2 m and porosity of 0.9, and all simulations used the same bed initial conditions. For the sediment classes input with river discharge, the settling velocities were determined in previous studies by calibration to observations of suspended sediment time series after discharge events [Ralston et al. 2013].

The model simulation periods span a range of forcing conditions, including extreme discharge events of Tropical Storms Irene and Lee in summer 2011 [Ralston et al. 2013], a typical spring freshet in 2014, and a lower discharge winter and spring in 2015 [Ralston and Geyer 2017]. Those simulations did not incorporate the wave model, as they were primarily focused on sediment transport in the Hudson River estuary where waves do not have a dominant role. For this study, we also examined the role of waves for sediment dynamics near Jamaica Bay by running the model for a period focused on Hurricane Sandy in fall 2012, comparing cases with and without the wave model. The SWAN model grid was the same as for ROMS. SWAN and ROMS were fully coupled, and the interval for data exchange was 20 min. Wind forcing was from the North American Mesoscale model (12-km resolution), and wave boundary conditions were interpolated from Wave-Watch III output.

Data from NOAA buoy 40025 located offshore 65 km southeast of Jamaica were used to assess wave heights offshore in the coastal ocean. Water level data was also used from the NOAA station 8518750 at The Battery in New York Harbor. We also used wind data from the North American Regional Reanalysis (NARR) for analysis of winds over a longer time period due to gaps in the wind data in the 40025 buoy record.

Results

Tidal Variability

Maximum depth-averaged tidal currents at the mooring location exceed 1 m/s during spring tide and are typically less than

Table 1 Sediment characteristics in model

Sediment class	Settling velocity (mm s^{-1})	Critical stress for erosion (N m^{-2})	Erosion rate (kg m^{-2} s^{-1})
Sediment initially in bed			
Medium sand	40	0.5	3e−4
Fine sand	5	0.1	3e−4
Medium silt	0.6	0.05	3e−4
Sediment input with river discharge			
Fine silt	0.2	0.05	3e−4
Very fine silt	0.01	0.05	3e−3

0.7 during neaps (Fig. 2b). Peak flood currents are modestly stronger than ebb currents due to the flood dominance of this system (Fig. 2b). Based on harmonic analysis applied to spring tide conditions, the semidiurnal tide has an amplitude of 1.06 m/s while the quarter and sixth diurnal motions have amplitudes of 0.09 and 0.11 m/s respectively (Table 2). However, it is phasing of quarter diurnal flows relative to the semidiurnal motion that augments the flood tide. This suggests that the flood dominance is associated with nonlinear advection [Parker 1991]. The tidal asymmetry in the depth-averaged currents corresponds to peak flood tide bottom stresses that are 20% higher than peak values during ebb.

The tidal asymmetry in bottom stress is even more pronounced when estimated with near-bottom currents (1.2 m above bottom (mab)). Using a drag law relationship with $C_D = 0.002$, flood stresses during spring tides approach 2 Pa, while during ebbs, maximum bottom stress is 1–1.5 Pa (Fig. 2c). Direct estimates of bottom stress from the ADV revealed a similar tidal asymmetry (Fig. 3a, b). The tidal asymmetry in stress is accompanied by a tidal asymmetry in suspended sediment concentration throughout much of the water column, with peak spring tide flood suspended sediment concentrations of 7–9 g/m^3 compared with ebb concentrations that are typically 5–6 g/m^3. During neap tide, suspended sediment concentrations remain low throughout the tidal cycle. A scatter plot of stress versus sediment concentration also reveals this tidal asymmetry and suggests a linear relationship between stress and SSC with a background level of 5 g/m^3 (Fig. 3b). We note that this background value falls on the high end of observed POM in the Hudson River plume [Malone and Chervin 1979], though this likely includes both wash load sediment and POC from Jamaica Bay.

The tidal asymmetry is also evident in tidally phase-averaged SSC during spring conditions from the moored observations (Fig. 3c). SSC is greater and sediment is suspended much higher in the water column on flood relative to ebb. The tidally phase-averaged currents also show greater near-bottom (1 mab) velocities on flood relative to ebb, with near-bottom currents exceeding 0.8 m/s during the flood while only reaching 0.7 m/s on ebb (Fig. 3c).

Table 2 Amplitude of tidal constituents from depth-averaged currents during spring tide condition (defined as times when the tidal amplitude is 1.2 times the mean tidal amplitude. Fit is to $U = A_i \times \sin(\omega_i \times t + \theta_i)$ where A_i and θ_i are the amplitude and phase of the ith tidal component respectively. Time is in days and reference to Jan 1, 0000

Constituent	Amplitude (m/s)	Phase (degrees)
M2	1.068	− 43.2
M4	0.090	145.45
M6	0.111	− 167.05

Cross-sectional structure of salinity, velocity, and SSC from the spring tide shipboard surveys also exhibited elevated currents and SSC on flood relative to ebb (Fig. 4). Spring tide currents exceed 1.2 m/s near-surface over the thalweg and weaken near the bed and over the flanks of the channel (Fig. 5a). During the ebb tide, there is weak stratification over the northern half of the thalweg with the halocline located near 7-m depth (Fig. 4a). SSC is generally less than 10 g/m^3 across the entire section (Fig. 4b). During the flood tide, stratification is weak (Fig. 4c) and SSC is greater during the flood, relative to ebb approaching 20 g/m^3 near the bottom on the northern flank and is generally over 10 g/m^3 in most of the section (Fig. 4d).

Estimates of the instantaneous along channel sediment flux were made for each of the 24 cross-channel surveys (Fig. 6). Sediment fluxes showed tidal asymmetry, with flood tide fluxes remaining close to 5×10^4 g/s for over 1 h while ebb sediment fluxes reached a maximum of 4.5×10^4 g/s and fell off more rapidly than on flood. Least-squares fit to mean transport and transports at the M2, M4, and M6 tidal frequencies place the mean transport at 3 kg/s, which if occurring during spring tides only (50% of the time) corresponds to 45 kt/year.

Subtidal Variability

Subtidal variability in sea level that occurs in the 2–5-day weather band is enhanced in the winter months (Fig. 2a) consistent with previous studies in the region [Wong and Wilson 1984]. Subtidal variability in the estuarine shear flow ($u1$) can be quantified by the surface to bottom velocity difference of $u1$, which we call Δu. $u0$ exhibits variability in the 2–5-day weather band that, like the sea-level data, is more energetic in the winter months (Fig. 2d). We attribute this low-frequency variability to coastal set-up. $u0$ also has a full-record mean inflow of 0.025 m/s. This mean inflow is consistent with the shipboard survey that shows a mean inflow over most of the section of 0.02–0.05 m/s but with a strong outflow of over 0.1 m/s in the southern 100 m of the section (Fig. 5b). These flows are much larger than the flow due to the mean freshwater discharge to the system which is on the order of 0.001 m/s. Therefore, the 0.025 m/s mean inflow observed at the mooring site reflects lateral shear in the mean flow and must be compensated by outflow in other parts of the channel.

The low-frequency sheared flow (Δu) is generally negative and consistent with estuarine exchange flow, with more landward (eastward) flow at depth than at the surface (Fig. 2d). Similar to $u0$, Δu has synoptic-scale variability that is more energetic in the winter months, indicating that it also is modified by the meteorological forcing. However, Δu is almost always negative and has a mean value of − 0.04 m/s. This mean shear combined with the mean vertical structure of the suspended sediment (Fig. 3c) also results in a net transport of

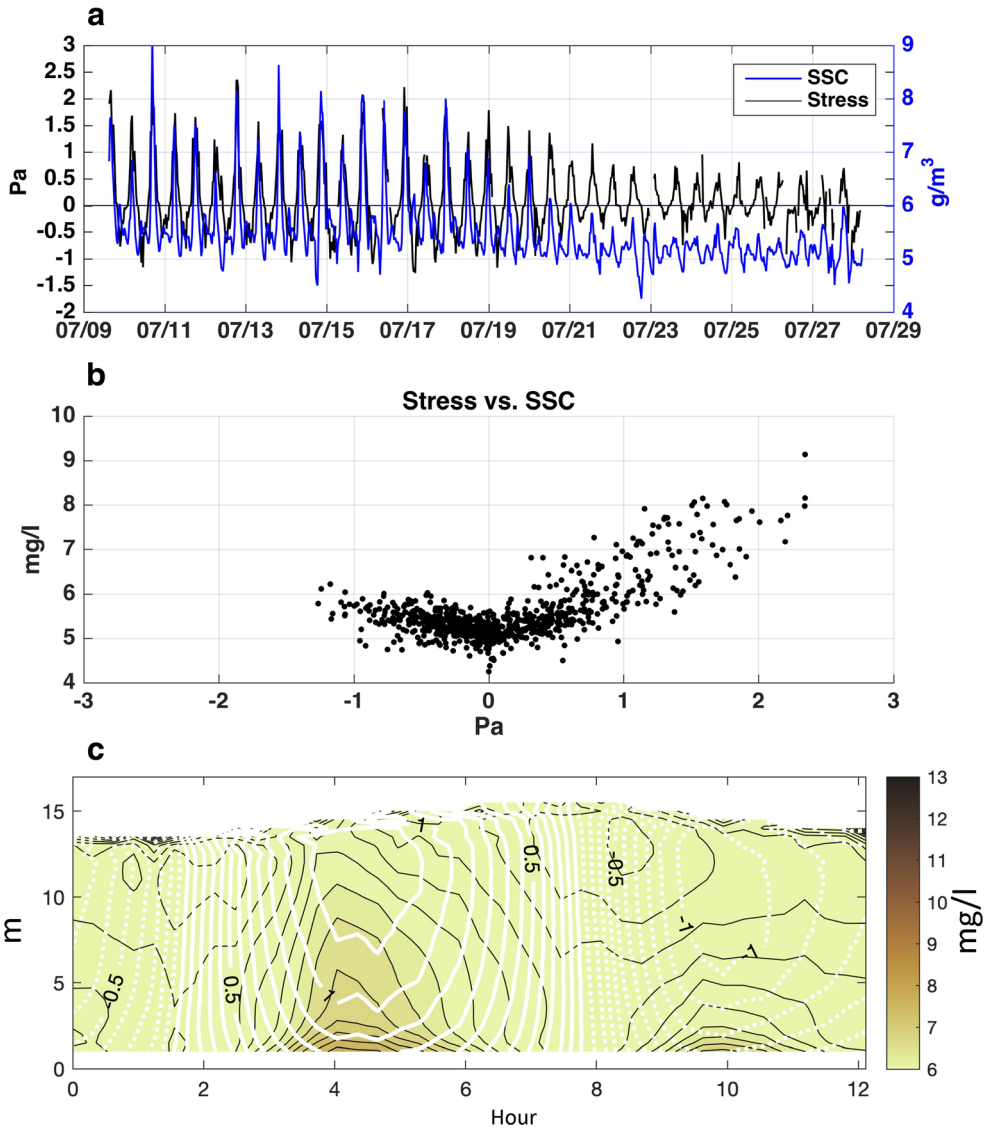

Fig. 3 **a** Bottom stress estimated with eddy covariance method with ADV (black) and near bottom TSS (blue). **b** Stress vs TSS. Flood is positive. **c** Tidal phase average of along channel velocity (white contours) and TSS (brown and black contours) from ADCP. Slack water is indicated by thick grey lines. Numbers on contours are for velocity

sediment into the bay. However, as will be shown later, the sediment transport driven by the mean shear is significantly less than that driven by tidal variability, and together are greater than the export associated with $u0$ to suggest a net sediment flux into the bay.

Sediment Flux

Time series of the sediment flux estimates from the bottom moorings, fixed bridge sensors, and the shipboard surveys all show elevated fluxes into Jamaica Bay on flood relative to ebb (Fig. 7b). All the observational methods also show strong spring-neap variability, with greater landward transport during spring tides. However, there are clear episodes of increased landward transport in the bridge-based measurements that are not evident in the bottom mooring data. In particular, during times of elevated significant wave heights in the ocean (Fig. 7a), suspended sediment flux measured at the bridge site increases substantially more than indicated by the moored observations. This is most notable during the winter months when storms are more frequent and also during October 2015 when Hurricane Joaquin passed offshore of the region and produced offshore significant wave heights that exceeded 4 m. The increase in sediment flux measured at the bridge site is due to elevated suspended sediment concentration detected by the OBS rather than changes in current velocities. In contrast, the acoustic backscatter recorded by the moored AWAC did not capture the elevated TSS during storm events, suggestive of a change in particle size distribution during the wave events that we discuss in the model results section and the discussion.

Estimates of the annual sediment flux are made by integrating each of the sediment flux time series over time (Fig. 8). For the 462 days of the mooring deployment (21 May 2015 and 25 August 2016), we obtained 422 daily estimates of sediment flux. The missing data were filled with the mean daily sediment flux based on the 422 daily estimates. The

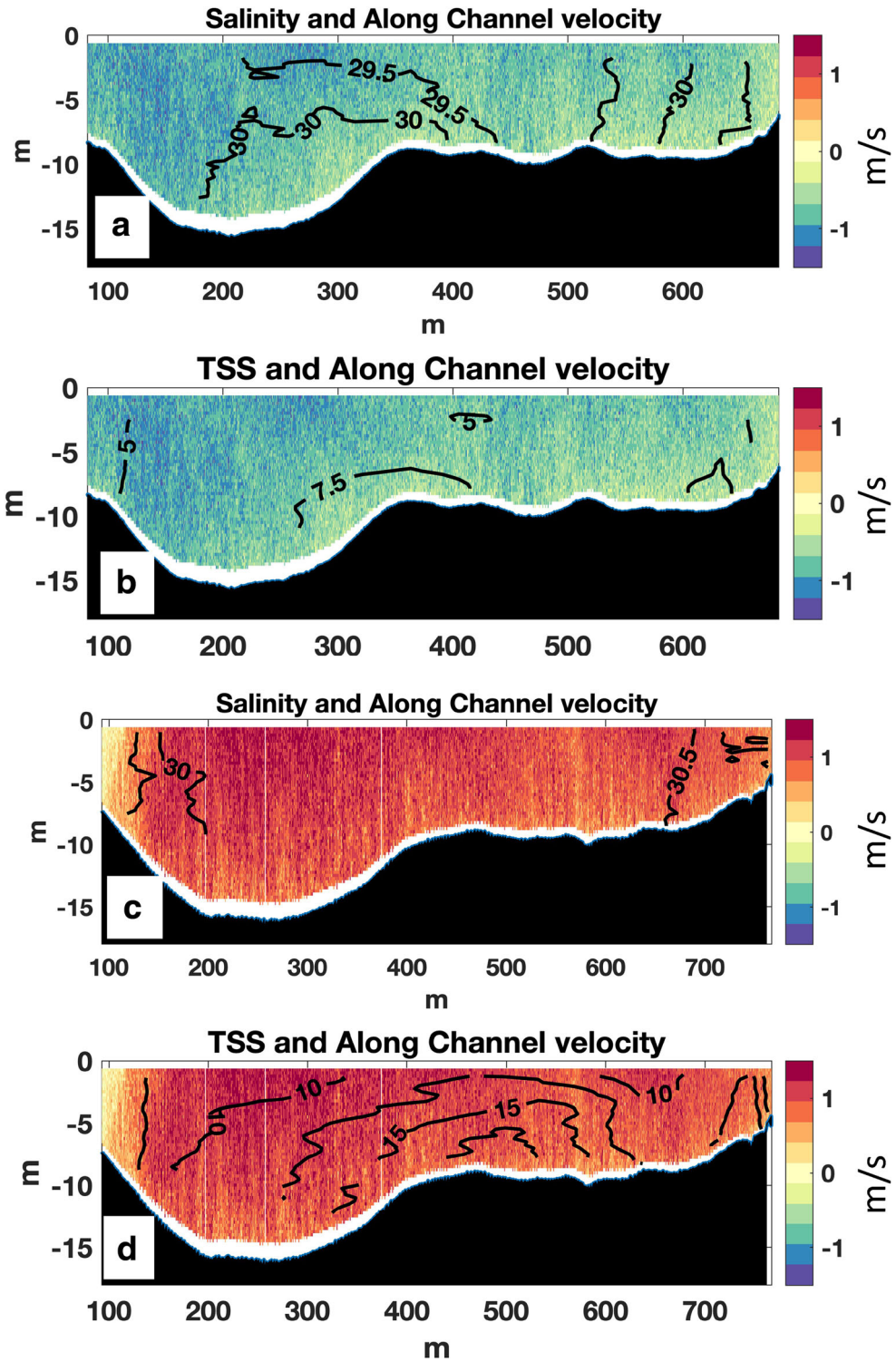

Fig. 4 **a** Salinity (contour) and along channel velocity (color) during maximum ebb. **b** Velocity (color) and TSS g/m^3 (contour) during maximum ebb. **c** Salinity (contour) and along channel velocity (color) during maximum flood. **d** Velocity (color) and TSS g/m^3 (contour) during maximum flood. Perspective of figures is looking out of the bay with the north to the right

cumulative sediment flux based on the mooring is equal to 36 kt/year, while the bridge station estimate is 55 kt/year. These measurements compare favorably to the radionuclide based estimate of sediment supply by Renfro et al. (2016) of 74 kt/year based on ^{210}Pb but considerably less than their estimate of 390 kt/year based on ^{234}Th.

Model Analysis

The domain of the circulation and sediment transport model used here spans the Hudson River estuary, New York Harbor, and the surrounding region, and while it was not developed specifically for this study, we can use it to assess how the

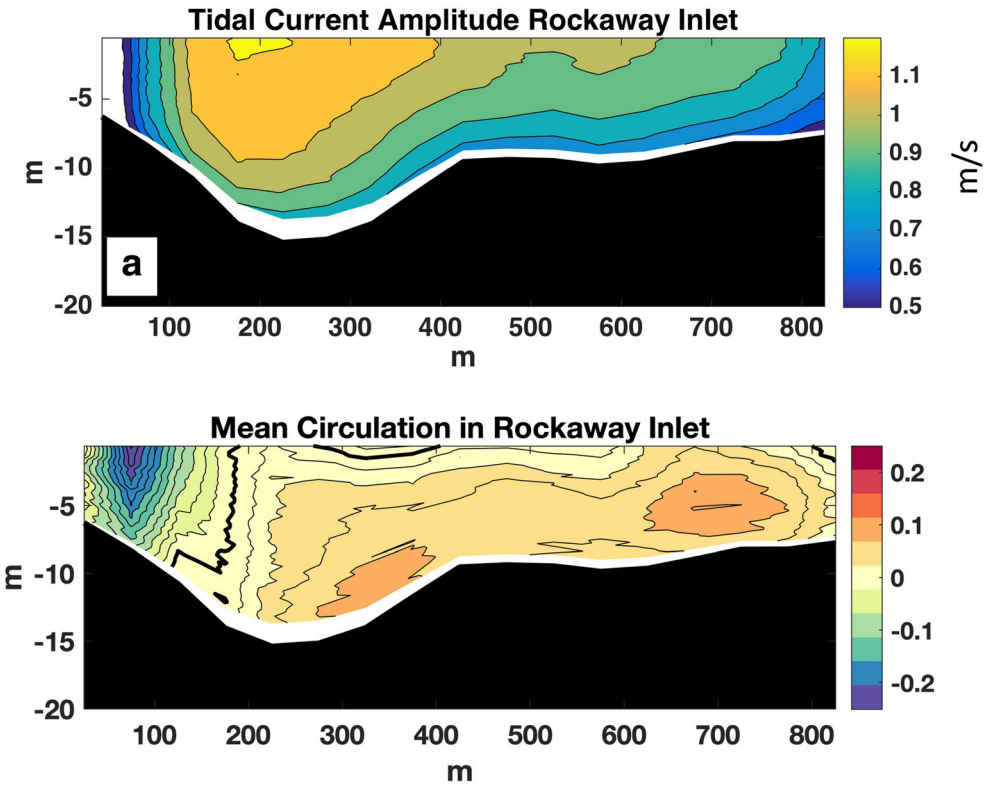

Fig. 5 **a** Amplitude of semidiurnal along channel currents from tidal cycle survey. **b** Mean along channel flow from tidal cycle survey/perspective of figures is looking out of the bay with the north to the right

sediment fluxes into Jamaica Bay fit into the regional setting. The model is also used to examine how variability in forcing factors like river discharge and waves affect the calculated sediment transport to Jamaica Bay. The period of model simulation that overlaps with the observations is about 5 months from November 2014 through April 2015. The cumulative sediment flux in the model has similar magnitude and temporal variability as the observations, with an annualized average of 74 kt/year into Jamaica Bay (Fig. 7b). The average sediment flux rate over the full model period is slightly greater than calculated from the mooring or bridge observations, but an initially greater rate of sediment import in the model may be due to uncertainty in the bed sediment distribution offshore that remains despite the model spin-up. Not including the first month of the simulation, the average import rate over the remainder of the 2015 simulation is 53 kt/year. As in the moored observations, the transport into Jamaica Bay in the model is strongly tidally driven, with increased import during spring tides and tidal pumping as the dominant mechanism of transport into the bay as is apparent in Fig. 3a.

Jamaica Bay does not have a significant direct input of sediment from its local watershed, but its location near the mouth of the Hudson River provides a major potential source of fine sediment for import. The tidal Hudson extends about 250 km north of Jamaica Bay, where the two major rivers contributing freshwater sediment to the system converge, the Mohawk and Upper Hudson Rivers. Event-scale, seasonal, and interannual variability in river discharge corresponds with even greater temporal variability in the sediment input from the rivers [Ralston and Geyer 2017; Ralston et al. 2013].

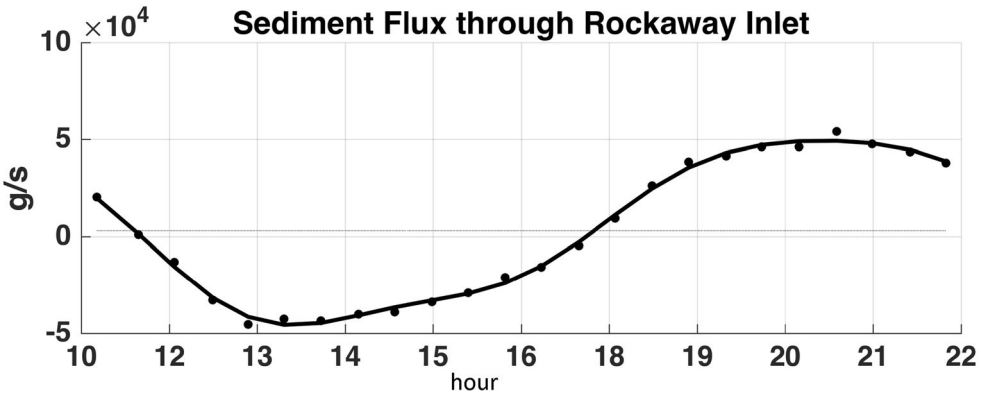

Fig. 6 Sediment flux through Rockway Inlet measured over tidal cycle during spring tide conditions. Dots show direct estimates. Black line is least squares fit to an M2, M4, and M6 signal plus a mean. The grey line just above zero is the mean value and equal to 3 kg/s

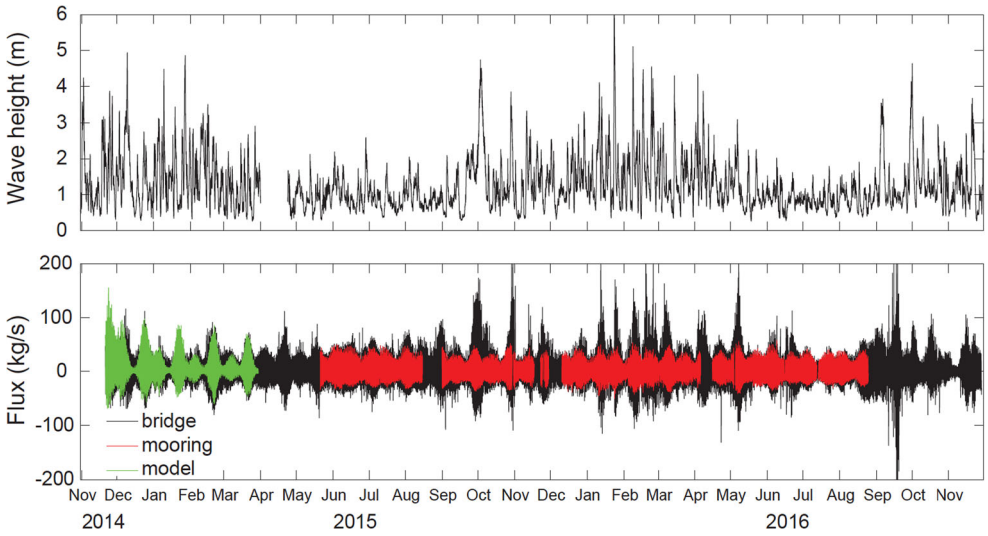

Fig. 7 **a** Significant wave height in coastal ocean (from NOAA Buoy 40025). **b** Estimates of sediment flux from mooring (red), bridge monitoring station (black), and modeled (green)

Model results spanning a wide range of discharge conditions are evaluated to assess the connection between sediment inputs to the Hudson estuary and transport into Jamaica Bay.

The previously discussed simulation period from early 2015 was a winter and spring period, but the discharge from the Upper Hudson and Mohawk during this period was much less than typical for that season (Fig. 9). The previous year's spring freshet (2014) included several large discharge events and was more representative of the seasonal increase in freshwater and sediment inputs. Extreme discharge events were also simulated, including summer 2011 when Tropical Storms Irene and Lee produced two of the highest discharges on record. In contrast, Hurricane Sandy in 2012 brought little rain to the watershed, and discharge remained near the climatological average.

The wide range of flow and sediment input to the Hudson estuary in the simulations corresponded with remarkably little variability in the sediment flux into Jamaica Bay (Fig. 9). In all the cases, the dominant variability was spring-neap, with enhanced sediment import during spring tides, and the long-term trends of sediment import were similar at time scales of a few months or greater. The model was also used to track sediment input from the watershed during the simulation separately from sediment initialized on the bed. Rather than recent watershed inputs from the spring freshet, the sediment imported to Jamaica Bay comes from remobilized bed sediment. After

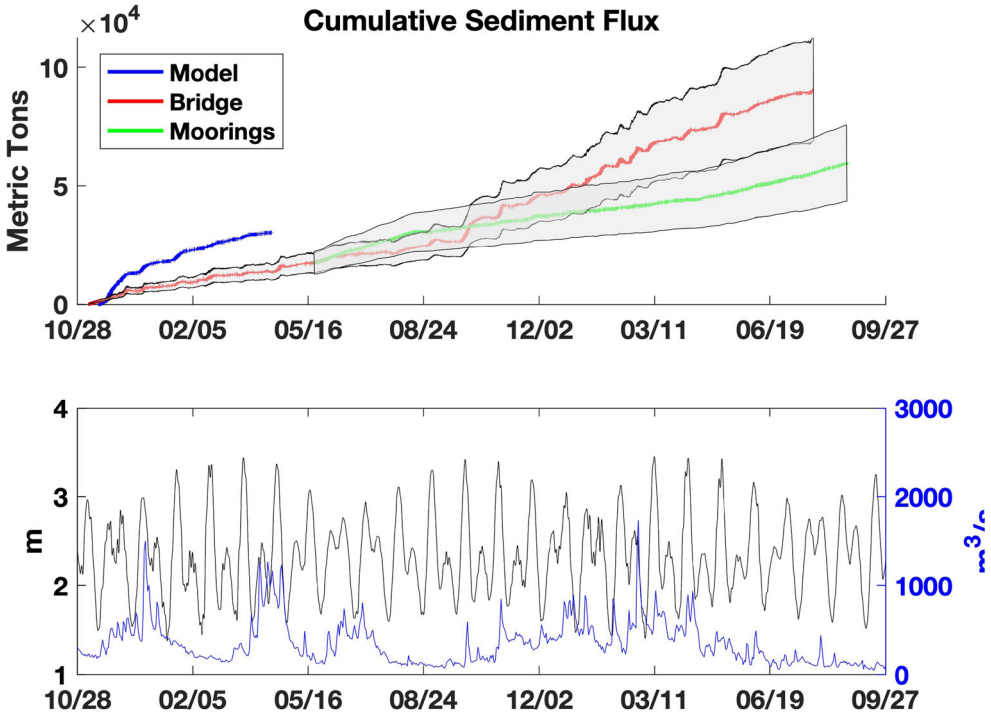

Fig. 8 Top panel: integration of net sediment flux through rockaway inlet from the model (blue), bridge station (red), and mooring (green) with error estimates (grey). Bottom panel: tidal range (black) and Hudson River discharge at Green Island (USGS01358000) (blue). Error estimates on sediment flux are based on the RMS error of the prediction of SCC is relative to the mean value of the SSC. For the bridge station, this was 27% and 22% for the moored site

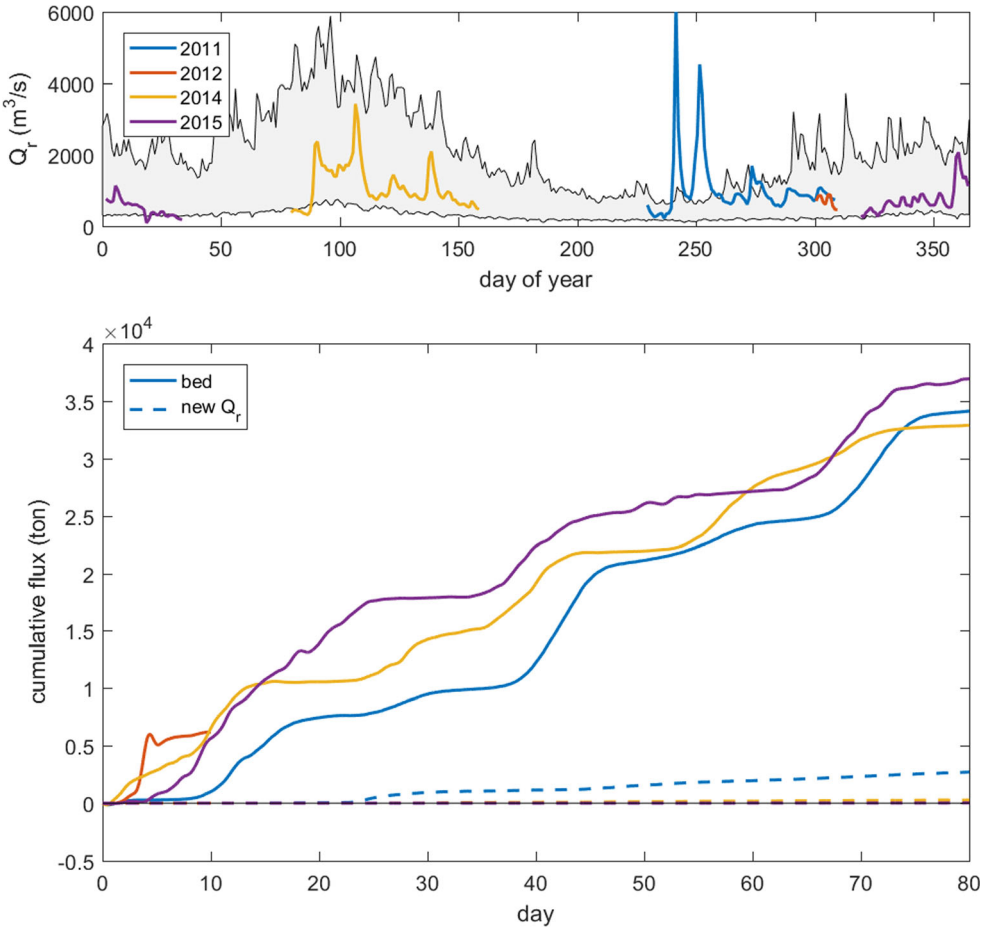

Fig. 9 (Top panel) Combined discharge from the Upper Hudson and Mohawk Rivers vs. day of year during the four simulation periods, with the climatological 5th and 95th percentile discharges. (Bottom panel) Cumulative sediment flux into Jamaica Bay during the four simulation periods. Dashed lines show the sediment flux associated with input from all rivers during the simulation period. The peaks in river flow in 2011 (blue line top panel) are associated with Hurricanes Lee and Irene

the massive sediment inputs from Irene and Lee, new sediment from the rivers represented about 15% of the total imported, but in all other cases, the travel time for sediment from the watershed to the mouth of Jamaica Bay is much longer than the simulation period of several months [Ralston and Geyer 2017].

An important exception to the predominance of the tides in the model time series of sediment flux was for 2012 with Hurricane Sandy, which had a brief but large increase in sediment import. As seen in the observations in 2016 with Hurricane Joaquin, wave-driven resuspension increased suspended sediment concentrations offshore of Rockaway Inlet, increasing the import during flood tides. Wave-driven resuspension inside of Jamaica Bay is less than outside the bay due to the limited fetch for local generation and deep navigational channels, so the tidal asymmetry in transport is enhanced, and based on model results, the sediment import to Jamaica Bay associated with Hurricane Sandy was 2.4 times greater including wave effects than the model without waves (Fig. 10). The differences in transport only lasted for a few days, but including the waves made the sediment during the rising limb of the storm surge greater than the export during the retreat of the storm surge, resulting in significant net import.

Discussion

Implications of Sediment Flux for Morphological Evolution

With the substantial hardening of Jamaica Bay's watershed and coastline, we assume that the sediment supply to the bay is primarily of marine origin, consistent with the results of Renfro et al. (2010) based on elevated levels of ^{234}Th near Rockway Inlet. Therefore, the estimates of net sediment transport through Rockaway Inlet represent an estimate of the total supply of sediment to the bay. One question fundamental to the trajectory of the wetlands in Jamaica Bay is whether the calculated sediment supply is sufficient to keep pace with sea-level rise. To quantitatively assess this, we use the following simple sediment budget:

$$Sf_{\mathrm{eq}} = R(A_m\rho_m + A_{\mathrm{st}}\rho_{\mathrm{st}}) \quad (6)$$

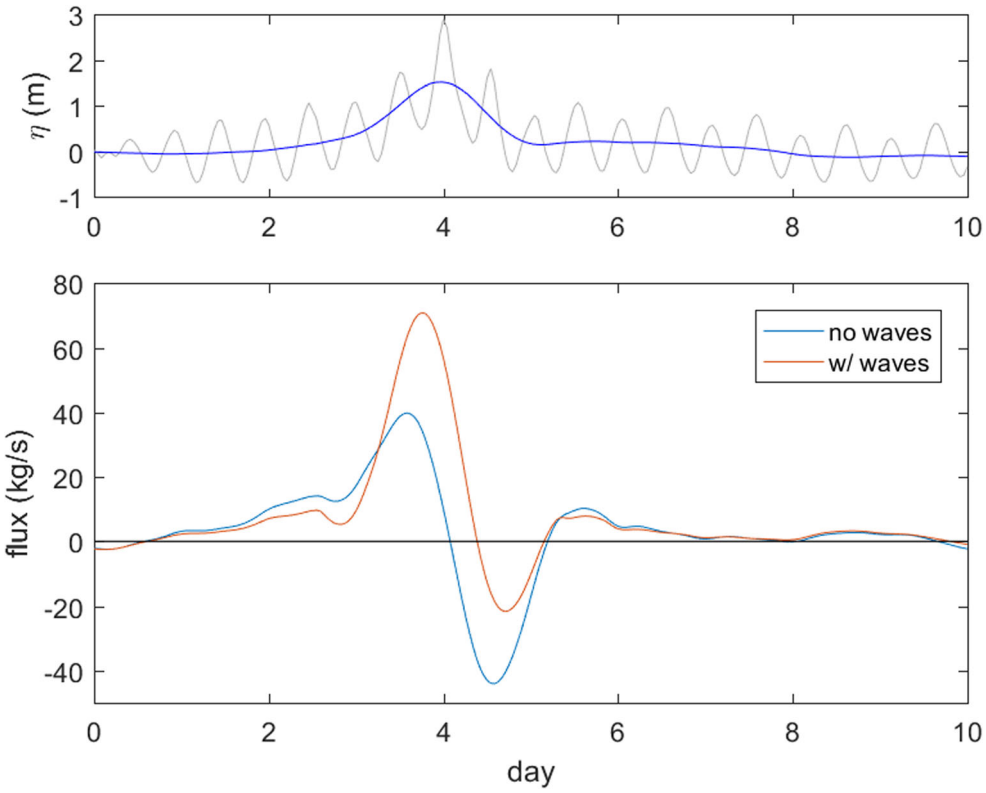

Fig. 10 Model results from Hurricane Sandy in 2012. (Top) Hourly and low passed water level time series in Rockaway Inlet. (Bottom) Sediment flux at Rockaway for model simulations with wave forcing and without

where Sf_{eq} is the required sediment flux to keep up with sea-level rise, R is the rate of relative sea-level rise in Jamaica Bay, A_m and A_{st} are the marsh and subtidal areas of the bay, and ρ_m and ρ_{st} are the bulk densities of sediment in the marsh and subtidal areas. If Sf_{eq} is greater than the supply of sediment through Rockaway Inlet, then we could conclude that the bay's morphology will be unable to keep up with sea-level rise and point to the lack of sediment as a contributing factor to the loss of marsh in Jamaica Bay. In contrast, if Sf_{eq} is less than the supply of sediment then we could conclude that there is a sufficient supply to keep pace with sea-level rise and the loss of wetlands is primarily due to other factors. The relative rate of sea-level rise at the Battery in New York Harbor is estimated as 3.38 mm/year over the period 1975–2014 based on NOAA observations. Sea-level rise, however, at coastal plain sites are 0.3–1.3 mm/year higher than at bedrock locations (The Battery) due to groundwater extraction and soil compaction [Miller et al. 2013], suggesting that relative sea-level rise in Jamaica Bay is 3.68–4.68 mm/year. Subtidal and marsh area are reported as 39 km^2 and 3.5 km^2 respectively, and we assume $\rho_s = 700$ kg/m^3 [Renfro et al. 2010] and $\rho_m =$ 310 kg/m^3 [Morris et al. 2016] respectively. While there is considerable uncertainty in marsh density [Morris et al. 2016], the marsh surface only represents 4% of the total inorganic sediment budget of Jamaica Bay and does not significantly contribute to uncertainty in Sf_{eq}. Therefore, the rate of relative sea-level rise is probably the largest uncertainty in estimating Sf_{eq}. Using the above values, including the above range of sea-level rise, we calculate that $Sf_{eq} = 101$–129 kt/year. The mean value for Sf_{eq} is 1.3–4.7 larger than our estimates and is also greater than the estimates of sediment import by Renfro et al. (2010) of 74 ± 4.5 kt/year.

Marshes do have the ability to maintain their vertical position through autochthonous production, and recent studies suggest they can outpace sea-level rise [Hopkinson et al. 2018; Kirwan et al. 2016]. However, the net sediment deficit relative to sea-level rise for the entire bay suggests that channels and flats will deepen, thereby creating accommodation space that may be filled by lateral loss of marsh material. While lateral marsh loss may contribute to vertical marsh accretion, lateral marsh loss results in a decrease of marsh area because all of the marshes in the bay are either isolated islands or their landward extent affronts hard urban infrastructure.

Even if the supply of sediment to the bay exceeds Sf_{eq}, for the marshes to keep up with sea-level rise, sediment entering the bay must reach the top of the marsh platform. Given the depth of the main channels and the general weakening of tidal currents in the interior of the bay, much of the sediment transported into the bay through the energetic inlet would be preferentially deposited in the main channels rather than the marsh platforms. Indeed, the Renfro et al. (2016) estimate of 76 kt/year assumed that sediment accumulation only occurred in the muddy regions that represent only 40% of the subtidal region and tend to be deeper. The fact that our estimate is in agreement with theirs suggests that the bulk of sediment supplied to the bay is indeed deposited in the subtidal region.

Therefore, we suggest that for the marsh platforms to keep up with sea-level rise, the sediment supply must exceed Sf_{eq}. Moreover, the sediment supply will become increasingly insufficient for marsh stability given the expected acceleration in sea-level rise in the coming decades/centuries.

Next, we apply 6 to the bay's configurations in 1907 reported to be $A_m = 65$ km^2 and $A_{st} = 35$ m^2 in 1907 [Hartig et al. 2002]. Assuming, like in the modern case, a local subsidence rate of 1 mm/year places relative sea-level rise in the bay at 3 mm/year [Kemp et al. 2017]. Equation 6 then indicates, given the 1907 configuration, Sf_{eq} = 132 kt/year. Interestingly, this is not significantly different than Sf_{eq} in today's system despite the total area of the bay reduced by nearly 50% due to land reclamation (primarily associated with what is today's JFK airport). Rather, Sf_{eq} has remained relatively constant because the required supply of sediment per unit area has increased as the bay transitioned from mostly marsh, which requires little sediment per unit area, to mostly subtidal areas that require significantly more sediment supply to keep up with sea-level rise. While we do not know if the bay was maintaining equilibrium in the late nineteenth and early twentieth century, dredging of the bay began in the nineteenth century, and by 1930, marsh islands had disappeared [Black 1981], indicating that marsh loss was active in the early twentieth century. This is also consistent with the reduction of the marsh area to 16 km^2 by 1970 [Hartig et al. 2002]. Furthermore, we note that the acceleration of sea-level rise from a regional background rate of 1 mm/year, associated with glacio-isostatic adjustment, began around 1800 [Kemp et al. 2017]. This suggests that our estimated sediment supply would exceed Sf_{eq} in the early to mid-nineteenth century and only in the late nineteenth century did this estimate fall below $Sf_{eq.}$ The combined effect of intense local anthropogenic deepening of the bay, loss of marsh islands, and an acceleration of sea level has acted to increased Sf_{eq} in recent centuries. Nevertheless, future increases in sea-level rise will only increase Sf_{eq} further. Note, however, that the supply of marine sediment to the bay must have been influenced by dramatic changes in inlet configuration over the past few centuries [Sanderson 2016], but estimating this change is beyond the scope of this work.

Constraining Uncertainty in Sediment Fluxes with Multiple Methods

The observational methods presented here have complementary strengths and weaknesses in spatial resolution and temporal coverage. The instruments on the seafloor mooring resolve the vertical structure of velocity for an extended period, but only at one location in the channel cross-section. Moreover, the acoustic backscatter is less responsive to finer sediments and appears to underestimate sediment fluxes during coastal storm events when waves resuspend fine sediment from the sea-bed. The bridge-mounted sensor measures the lateral structure across the channel and the shipboard surveys resolve both vertical and lateral velocity structure, but are limited in duration.

These four methods that together have a mean value of 55 kt/year of sediment flux into the bay with a standard deviation of 31 kt/year. The Student t statistic for one-tail 95% confidence puts the upper limit at 86 kt/year, which is slightly less than our lower bound estimate for Sf_{eq} indicating that sediment flux through Rockaway inlet is insufficient to keep up with sea-level rise. Based on two sediment cores taken from marshes in Jamaica Bay, Peteet et al. (2018) found that the marsh platform is keeping up with sea-level rise, but that the inorganic fraction of the marsh platform decreased from 60% deeper in the core (1650–1900 CE) to 30–40% in the more recent deposits. This decline in inorganic material is consistent with our observations of a limited supply of sediments and with the estimate of the marsh density, although it also may reflect a difference in position of the marsh relative to MSL and/or distance to the Bay. However, most of the estuary is comprised of subtidal channels whose sediments have a much higher bulk density and averaged over their total area will not be able to keep up with sea-level rise. The accumulation of material on the marsh platform has occurred during a time of rapid erosion of the marsh edges suggesting that some of the material deposited on the marsh platform may originate from the marsh itself. Thus, while the platform may keep up with sea-level rise, the marsh area decreases over time.

Sediment Transport Mechanisms

Estimates of the estuarine shear (F_1) and tidally pumping (F_2) sediment fluxes indicate that over 95% of the transport during this time period is associated with tidal sediment flux. Tidal sediment flux also exhibits strong spring/neap variability (Fig. 11a) with most of the net flux occurring during spring tide. During spring tide, defined as times when the tidal amplitude exceeds 1 m, tidal pumping fluxes average 2.9 g/m/s and exceed 4 g/m/s at times, but during neap tide conditions, they are reduced to near zero. The mean value over this record is 1.5 g/m/s. In contrast, the mean value of F_1 is 0.033 g/m/s.

Next, we demonstrate that the above estimates of sediment flux are consistent with a simple model of sediment flux generated by the combination of the mean sheared exchange flow acting on the mean and vertically varying sediment concentration, and of a tidal flow acting on tidally asymmetric suspended sediment concentration. For the exchange flow sediment flux, we model the flow and the suspended sediment concentration as

$$u1(z) = \alpha_1 \left(z - \frac{H}{2} \right) \tag{7}$$

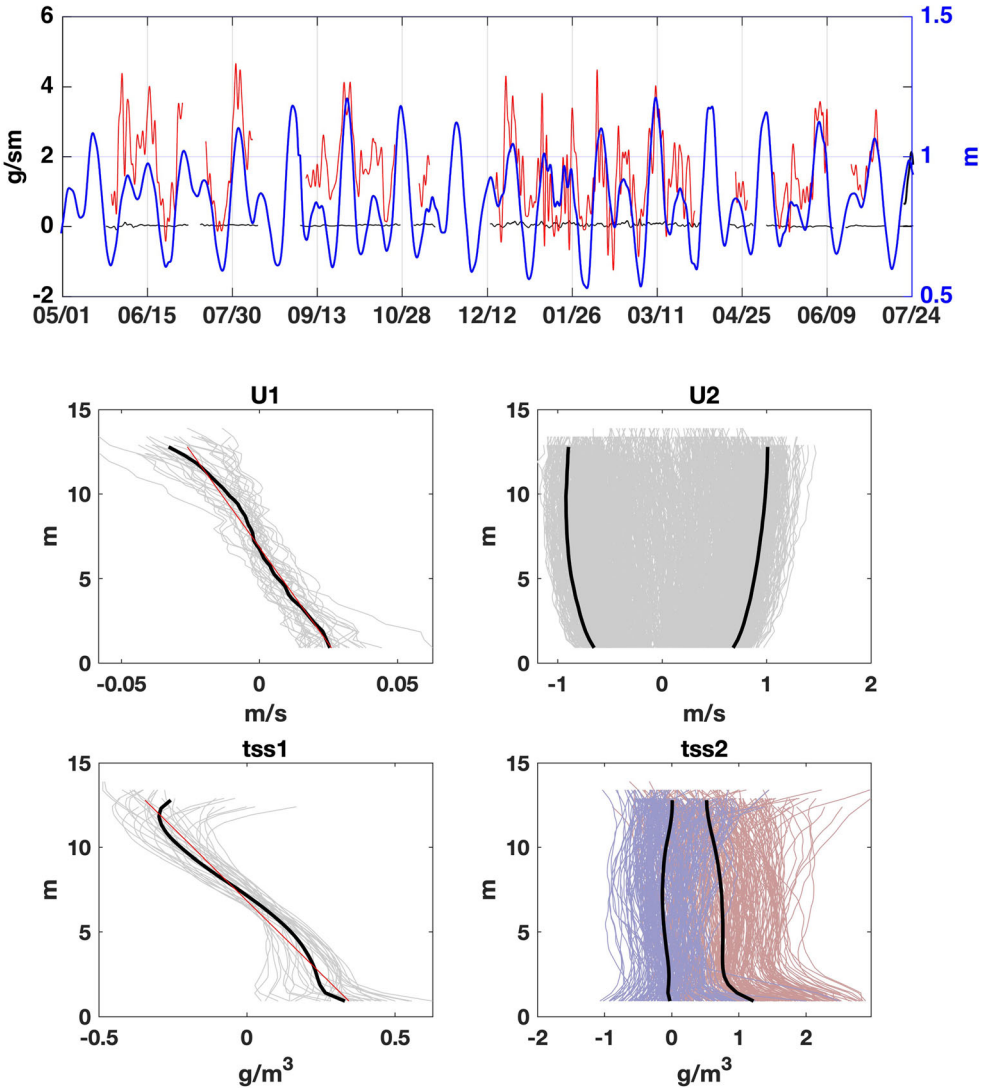

Fig. 11 Top Panel: tidal amplitude (blue), sediment flux associated with tidal pumping (red), and exchange flow (black). Lower 4 figures show data from July 10 to Aug 30, 2015, deployment. Middle two panels show vertical structure of the exchange flow (plotted daily) and the mean exchange flow (thick line) (left) and hourly high passed flows with thick line the mean profile for times that along channel depth averaged flows exceed 0.75 m/s. Lower left panel shows the low-frequency vertical structure of TSS plotted daily with the thick line the mean value. Lower right panel shows tidal variability with red showing flood, blue ebb, and the thick lines the mean value for strong floods ($u \geq .75$ m/s) and strong ebb ($u \leq -0.75$ m/s)

$$Tss1(z) = \alpha_2\left(z - \frac{H}{2}\right) \tag{8}$$

where α_1 and α_2 are the vertical gradient of the mean flow and suspended sediment concentration respectively. Note that the observations support this linear relationship with depth (Fig. 11). The flux (F_1) of sediment is obtained by integrating the product of (7) and (8) vertically, i.e.,

$$F_1 = \alpha_1 \alpha_2 H^3/12 \tag{9}$$

Based on linear regression of vertical profiles of the mean shear and suspended sediment concentration (Fig. 11), we estimate $\alpha_1 = 0.0044$ s^{-1}, $\alpha_2 = 0.058$ gm^{-4}, and $H = 12.5$ m (the depth over which these estimates are made). Using these values in Eq. (9) yields a value of 0.036 g/m/s, close to the direct estimate of 0.033 g/m/s above.

A model for sediment fluxes associated with tidal motion is based on the observations that tides and suspended sediment concentrations are largely in phase (Fig. 3) and that flood tide sediment concentrations are elevated relative to ebb tide. Another simplifying assumption is that tidal currents are purely semidiurnal (neglecting asymmetries) with amplitude U_T. The model includes a tidal asymmetry in suspended sediment concentration with a maximum flood concentration of C_f that exceeds the maximum value on the ebb, C_e. With this model, the tidal-driven sediment flux averaged over the tidal cycle is

$$F_2 = \frac{H}{T}\left[\int_0^{T/2} U_T C_f \sin^2(\omega t)dt - \int_{T/2}^{T} U_T C_e \sin^2 dt\right] = H\frac{U_T \Delta C}{4} \tag{10}$$

where T is the tidal period, ω the tidal frequency, and $\Delta C = C_f - C_e$. Applying (10) to spring tide conditions when ΔC is 0.80 g/m^3 (Fig. 11) and $U_T = 1.15$ m/s (the mean tidal current amplitude during spring tide) yields $F_2 = 2.78$ g/m/s, which is consistent with the direct estimate of tidal fluxes made at the mooring during spring tide.

The sediment transport driven by the mean sectionally averaged flow due to the freshwater discharge to the system (1.25 mm/s) times the mean suspended sediment concentration (5 g/m^3) exports 0.09 g/ms in 15 m of water. This is larger than the import by the exchange flux but less than the landward tidal flux. The mean freshwater discharge to the Bay of 10 m^3/s acting on a mean sediment concentration of 5 g/m^3 exports an annual load of 15 kt; however, this may be high organic matter associated with marsh detritus, plankton, and organics associated with wastewater discharge into the bay. However, the mean shear, presumably due to the horizontal density gradient, plays a role in enhancing bottom stress, which elevates SSC, on flood. Thus, the freshwater discharge into the bay may play an important role in the elevated stress on flood tide and the tidal transport of sediment into the bay. Nevertheless, in summary, tidal pumping is the dominant mechanism driving tidal fluxes through Rockaway Inlet.

While both the moored and bridge instrumentation showed a net inflow of sediment into the bay with significant spring/neap variability, the two estimates of sediment fluxes diverged during storm events when the OBS data indicated significantly higher suspended sediment loads than the AWAC backscatter data. We interpret this result as due to a change in the grain size of the suspended particulate matter. Acoustic backscatter increases with the cube of sediment size [Hoitink and Hoekstra 2005], and thus, the insensitivity of the Doppler to elevated suspended matter during storms would be consistent with finer grain material in the water column. We speculate that fine-grain material on the continental shelf is resuspended by the wave action and transported into the bay. In contrast, during low wave energy periods, sediment transport into the bay is dominated by locally resuspended sediments by tidal currents in the vicinity of the inlet. Since these local sediments are largely sand, an increase in fines from further offshore during storm events would cause a divergence between the ABS (AWAC) and OBS measurements, with the ABS underestimating the sediment flux. This suggests, therefore, that storm events may represent a mechanism to import fine-grain sediments to the bay [Castagno et al. 2018].

Sediment flux estimates from the bridge and moored stations increasingly diverge with increased offshore wave height conditions (Fig. 12a). For wave heights 1–1.5 m or less, which occurs approximately 80% of the time, the two sites give similar estimates of sediment flux. However, for wave heights greater than 1.5 m, the two estimates diverge, as the bridge estimate increases with wave height and the moored station remains relatively unchanged. Approximately 50% of the sediment flux at the bridge site occurred during periods when waves were greater than 1.5 m, despite this only representing 20% of the observation period (Fig. 12b). During the most extreme evens with waves exceeding 4 m, which represents storm conditions in this region, estimates at the bridge average 10 kg/s which corresponds to approximately 1.5 kt of sediment during a 2-day storm.

The Hudson River would be the likely source of fine-grain sediments that are initially deposited on the shelf following high river discharge events [Ralston et al. 2013] and are remobilized by waves during storms on the shelf and imported into Jamaica Bay. This delivery mechanism is consistent with sediment core analysis revealing the delivery of mineral-rich material to the marshes by the landfall of Hurricanes in Jamaica Bay over the past century [Clarke 2018]. This points to the importance of long term monitoring of sediment fluxes at the bay mouth due to the episodic nature of storm events.

To assess the frequency of storms during this study relative to the longer-term storm frequency, we compared the annual distribution of wind speed for years between 1980 and 2018 based on North American Regional Reanalysis (NARR) against that distribution during this study deployment. The analysis was performed on the grid point that was closest to Rockaway inlet (40 km SSE). We used this data set rather than observed winds from the National Buoy Data Center because of large gaps in 2015 and 2016 in the nearby offshore wind records (NBDC 44025 and 44009). Based on the NARR data, winds between 9 and 11 m/s occurred less frequently during the mooring deployment compared to the mean PDF over the 29-year record. For higher wind speeds, our study period is typical of the 29-year record (Fig. 13). Winds at speeds between 9 and 11 m/s occurred, an average of 621 h annually during our study, compared with to 766 h annually averaged over the full record. This corresponds to approximately 6 days or to 2–3 additional moderate wind events. However, winds exceeded 11 m/s for 444 h annually during our study compared to 448 h over the entire data set. Thus, we conclude that winds during the moored record, and thus wave-driven sediment resuspension, are typical of the longer-term record.

Both the observations and the model indicate that tidal pumping is the dominant mechanism driving sediment flux into Jamaica Bay. This is due to elevated bottom stress on flood tide, which is nearly twice as high as the bottom stress on ebb, and this results in higher suspended sediment concentrations on flood tide relative to ebb. Most of this asymmetry in stress is due to the superposition of the tidal flows with the estuarine circulation while ~20% of the elevated stress on flood is due to tidal distortion. Based on a quadratic drag law, the combination of a 1 m/s semidiurnal tide, a 0.09 m/s quarter diurnal tide, and a 0.04 m/s mean inflow produces a flood tide stress that is nearly 70% larger than the ebb tide stress.

Conclusions

Using a suite of moored observations, numerical modeling, and previous radionuclide estimates [Renfro et al. 2016], we

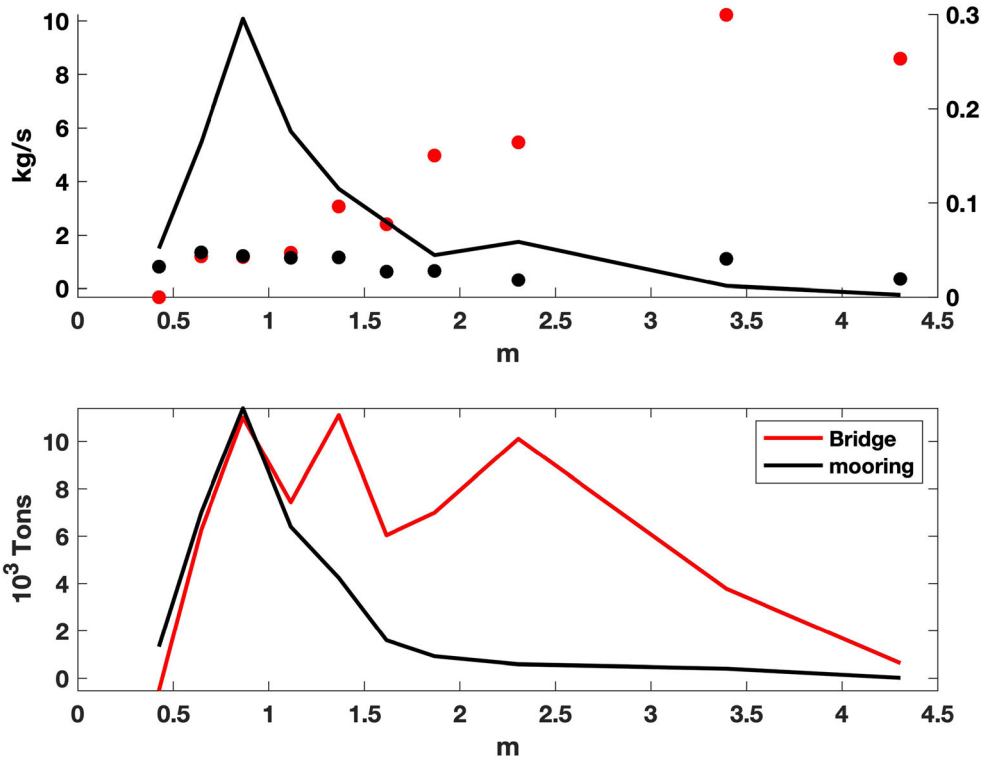

Fig. 12 Upper: distribution of wave height during sediment flux estimates (black line). Mean sediment flux as a binned by wave height for bridge estimate (red dots) and moored estimates (black dots). Lower: cumulative sediment flux as a function of wave height for bridge observation (red) and moored observation (black)

estimate that Jamaica Bay imports 55 ± 31 kt of sediment annually. This supply of sediment is less than our estimate of the supply required (Sf_{eq}) for the system to keep up with sea-level rise (101–128 kt/year). Moreover, due to the uneven distribution of sediment throughout the bay associated with the tendency for sediment to settle in deep channels and borrow pits rather than marsh platforms, we suggest that the system requires a sediment flux that exceeds Sf_{eq} for the entire

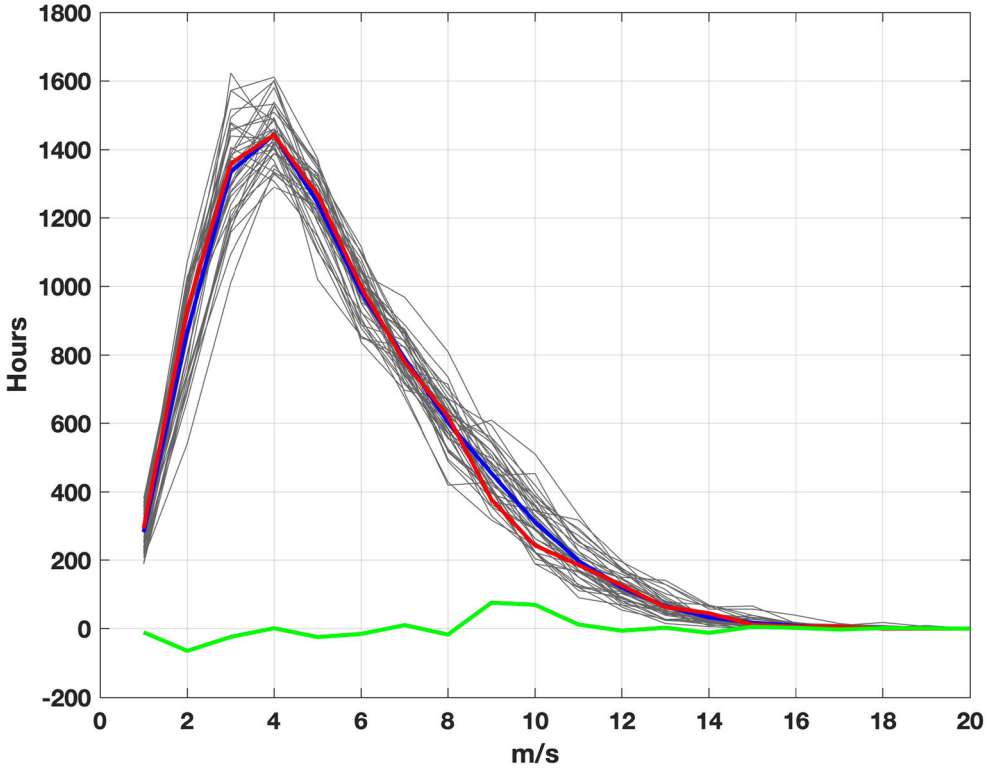

Fig. 13 Wind speed distribution of NARR data 40 km SSE of Rockaway Inlet. Black lines are distributions for individual years (1980–2018). Blue line is record mean annual distribution and red line is during this study on an annual basis. Green line is the difference between mean (blue) and this study (red)

bay-marsh system to keep up with sea-level rise. This is of particular concern given the predictions of accelerated rates of sea-level rise in the future. Sediment flux into Jamaica Bay is dominated by tidal pumping that is driven by a strong asymmetry in bottom stress due to a combination of tidal distortion and estuarine circulation. Sediment flux is strongly modulated over the spring/neap cycle with most of the sediment flux occurring over spring tide conditions. Sediment flux is enhanced by offshore wave activity that elevates the suspended sediment concentration that is imported into the bay, in particular for fine-grained sediment. Finally, with the upper bound of our estimate of sediment flux into the bay less than the lower bound Sf_{eq}, we conclude that it is likely that the supply of sediment to Jamaica Bay is insufficient for the marshes to keep up with sea-level rise. While other processes also likely contribute to wetland loss, such as eutrophication, we suggest that an insufficient sediment supply by itself would lead to a net sediment deficit and spatially averaged a deepening of the bay response to sea-level rise.

Acknowledgments Support for RJC was provided by the grant from the Department of Interior Hurricane Sandy Recovery program and from a National Science Foundation Coastal SEES grant (1325258). RJC thanks Elias Hunter and Chip Haldeman for their field and computational skills and Ken Roma for his dedication at the helm. Support for DKR was provided by NSF Coastal SEES award OCE-1325136. NKG, AES, RAC, and Marine Parkway data collection were funded by the USGS Coastal and Marine Geology Program and the Department of the Interior Hurricane Sandy Recovery Program (GS2-2D). The authors thank the three anonymous reviewers for their time and for helping us improve the clarity of this paper.

References

Barbier, E.B., S.D. Hacker, C. Kennedy, E.W. Koch, A.C. Stier, and B.R. Silliman. 2011. The value of estuarine and coastal ecosystem services. *Ecological Monographs* 81 (2): 169–193.

Barnard, P.L., D.H. Schoellhamer, B.E. Jaffe, and L. McKee. 2013. Sediment transport in the San Francisco Bay coastal system: an overview. *Marine Geology* 345: 3–17.

Benotti, M. J., I. Abbene, and S. A. Terracciano (2007), Nitrogen loading in Jamaica Bay, Long Island, New York: predevelopment to 2005 *Rep.* 2328–0328, Geological Survey (US).

Black, F. R. (1981), Jamaica Bay: a history, edited, US Department of Interior, Washington DC.

Boldt, J. A. (2015), From mobile ADCP to high-resolution SSC: a cross-section calibration tool, paper presented at 3rd Joint Federal Interagency Conference on Sedimentation and Hydrologic Modeling.

Booij, N., R. Ris, and L.H. Holthuijsen. 1999. A third-generation wave model for coastal regions: 1 Model description and validation. *Journal of geophysical research: Ocean* 104 (C4): 7649–7666.

Cartwright, R. A., and A. E. Simonson (2019), Estimating sediment flux to Jamaica Bay, New York Rep. 2328–0328, US Geological Survey.

Castagno, K.A., A.M. Jiménez-Robles, J.P. Donnelly, P.L. Wiberg, M.S. Fenster, and S. Fagherazzi. 2018. Intense storms increase the stability of tidal bays. *J Geophysical Research Letters* 45 (11): 5491–5500.

Chant, R.J., D. Fugate, and E. Garvey. 2011. The shaping of an estuarine superfund site: roles of evolving dynamics and geomorphology. *Estuaries and Coasts* 34 (1): 90–105.

Clarke, R. C. (2018) Vertical sediment accretion in Jamaica Bay Wetlands, New York, Louisiana State University and Agriculture and Mechanical College

Deegan, L.A., D.S. Johnson, R.S. Warren, B.J. Peterson, J.W. Fleeger, S. Fagherazzi, and W.M. Wollheim. 2012. Coastal eutrophication as a driver of salt marsh loss. *Nature* 490 (7420): 388–392.

Donatelli, C., N.K. Ganju, S. Fagherazzi, and N. Leonardi. 2018. Seagrass impact on sediment exchange between tidal flats and salt marsh, and the sediment budget of shallow bays. *Geophysical Research Letters* 45 (10): 4933–4943.

Edwards, T. K., G. D. Glysson, H. P. Guy, and V. W. Norman (1999), Field methods for measurement of fluvial sediment, US Geological Survey Denver, CO.

Fagherazzi, G., P. Mariotti, L. Wiberg, and K.J. McGlathery. 2013a. Marsh collapse does not require sea level rise. *Oceanography* 26 (3): 70–77.

Fagherazzi, S., G. Mariotti, P. Wiberg, and K. McGLATHERY. 2013b. Marsh collapse does not require sea level rise. *Oceanography* 26 (3): 70–77.

Fagherazzi, S., and A. Priestas. 2010. Sediments and water fluxes in a muddy coastline: interplay between waves and tidal channel hydrodynamics. *Earth Surface Processes and Landforms* 35 (3): 284–293.

Ford, M.A., D.R. Cahoon, and J.C. Lynch. 1999. Restoring marsh elevation in a rapidly subsiding salt marsh by thin-layer deposition of dredged material1. *Ecological Engineering* 12 (3–4): 189–205.

Friedrichs, C.T., and J.E. Perry. 2001. Tidal salt marsh morphodynamics: a synthesis. *J. Coastal. Res.* 7-37.

Ganju, N.K., Z. Defne, M.L. Kirwan, S. Fagherazzi, A. D'Alpaos, and L. Carniello. 2017. Spatially integrative metrics reveal hidden vulnerability of microtidal salt marshes. *Nature Communications* 8 (1): 14156.

Ganju, N.K., N.J. Nidzieko, and M.L. Kirwan. 2013. Inferring tidal wetland stability from channel sediment fluxes: observations and a conceptual model. *Journal of Geophysical Research: Earth Surface* 118 (4): 2045–2058.

Goodbred, S.L., Jr., and A.C. Hine. 1995. Coastal storm deposition: salt-marsh response to a severe extratropical storm, March 1993, west-central Florida. *Geology* 23 (8): 679–682.

Haidvogel, D.B., H. Arango, W.P. Budgell, B.D. Cornuelle, E. Curchitser, E. Di Lorenzo, K. Fennel, W.R. Geyer, A.J. Hermann, and L. Lanerolle. 2008. Ocean forecasting in terrain-following coordinates: formulation and skill assessment of the Regional Ocean Modeling System. *Journal of Computational Physics* 227 (7): 3595–3624.

Hartig, E. K., V. Gornitz, A. Kolker, F. Mushacke, and D. Fallon (2002), Anthropogenic and climate-change impacts on salt marshes of Jamaica Bay, New York City, Wetlands, 22(1), 71–89.

Hoitink, A., and P. Hoekstra. 2005. Observations of suspended sediment from ADCP and OBS measurements in a mud-dominated environment. *Coastal Engineering* 52 (2): 103–118.

Holdredge, C., M.D. Bertness, and A.H. Altieri. 2009. Role of crab herbivory in die-off of New England salt marshes. *Conservation Biology* 23 (3): 672–679.

Hopkinson, C.S., J.T. Morris, S. Fagherazzi, W.M. Wollheim, and P.A. Raymond. 2018. Lateral marsh edge erosion as a source of sediments for vertical marsh accretion. *Journal of Geophysical Research: Biogeosciences* 123 (8): 2444–2465.

Kemp, A.C., T.D. Hill, C.H. Vane, N. Cahill, P.M. Orton, S.A. Talke, A.C. Parnell, K. Sanborn, and E.K. Hartig. 2017. Relative sea-level trends in New York City during the past 1500 years. *The Holocene* 27 (8): 1169–1186.

Kim, S.-C., C.T. Friedrichs, J.P.Y. Maa, and L.D. Wright. 2000. Estimating bottom stress in tidal boundary layer from Acoustic Doppler Velocimeter data. *Journal of Hydraulic Engineering* 126 (6): 399–406.

Kirwan, M.L., and J.P. Megonigal. 2013. Tidal wetland stability in the face of human impacts and sea-level rise. *Nature Communications* 504 (7478): 53–60.

Kirwan, M.L., S. Temmerman, E.E. Skeehan, G.R. Guntenspergen, and S. Fagherazzi. 2016. Overestimation of marsh vulnerability to sea-level rise. *Nature Climate Change* 6 (3): 253–260.

Kopp, R.E. 2013. Does the mid-Atlantic United States sea level acceleration hot spot reflect ocean dynamic variability? *Geophysical Research Letters* 40 (15): 3981–3985.

Leonardi, N., N.K. Ganju, and S. Fagherazzi. 2016. A linear relationship between wave power and erosion determines salt-marsh resilience to violent storms and hurricanes. *Proceedings of the National Academy of Sciences* 113 (1): 64–68.

Malone, T.C., and M.B. Chervin. 1979. The production and fate of phytoplankton size fractions in the plume of the Hudson River, New York Bight. *Limnology and Oceanography* 24 (4): 683–696.

Mariotti, G., and S. Fagherazzi (2013), Critical width of tidal flats triggers marsh collapse in the absence of sea-level rise, Proceedings of the National Academy of Sciences, 201219600.

McSweeney, J.M., R.J. Chant, and C.K. Sommerfield. 2016. Lateral variability of sediment transport in the Delaware Estuary. *Journal of Geophysical Research: Oceans* 121 (1): 725–744.

Miller, K.G., R.E. Kopp, B.P. Horton, J.V. Browning, and A.C. Kemp. 2013. A geological perspective on sea-level rise and its impacts along the US mid-Atlantic coast. *Earth's Future* 1 (1): 3–18.

Morris, J.T., D.C. Barber, J.C. Callaway, R. Chambers, S.C. Hagen, C.S. Hopkinson, B.J. Johnson, P. Megonigal, S.C. Neubauer, and T. Troxler. 2016. Contributions of organic and inorganic matter to sediment volume and accretion in tidal wetlands at steady state. *Earth's future* 4 (4): 110–121.

Nitsche, F., W. Ryan, S. Carbotte, R. Bell, A. Slagle, C. Bertinado, R. Flood, T. Kenna, and C. McHugh (2007), Regional patterns and local variations of sediment distribution in the Hudson River Estuary, Estuarine, Coastal Shelf Science, 71(1–2), 259–277.

Parker, B. B. (1991), Tidal hydrodynamics, John Wiley & Sons.

Peteet, D.M., J. Nichols, and T. Kenna. 2018. Sediment starvation destroys New York City marshes' resistance to sea level rise [STUB]. *Proceedings of the National Academy of Sciences* 115 (41): 10281–10286.

Ralston, D.K., and W.R. Geyer. 2017. Sediment transport time scales and trapping efficiency in a tidal river. *Journal of Geophysical Research: Earth Surface* 122 (11): 2042–2063.

Ralston, D.K., W.R. Geyer, and J.C. Warner. 2012a. Bathymetric controls on sediment transport in the Hudson River estuary: lateral asymmetry and frontal trapping. *Journal of Geophysical Research: Oceans* 117 (C10).

Ralston, D.K., W.R. Geyer, and J.C. Warner. 2012b. Bathymetric controls on sediment transport in the Hudson River estuary: lateral asymmetry and frontal trapping. *Journal of Geophysical Research: Oceans* 117 (C10).

Ralston, D.K., J.C. Warner, W.R. Geyer, and G.R. Wall. 2013. Sediment transport due to extreme events: the Hudson River estuary after tropical storms Irene and lee. *Geophysical Research Letters* 40 (20): 5451–5455.

Reed, D. 2002. Understanding tidal marsh sedimentation in the Sacramento-San Joaquin delta, California. *J. Coastal. Res.* 36 (sp1): 605–611.

Renfro, A., J. Cochran, D. Hirschberg, and S. Goodbred (2010), Natural radionuclides (234Th, 7Be and 210Pb) as indicators of sediment dynamics in Jamaica Bay, New York *Rep.*, Natural Resource Technical Report NPS/NERO/NRTR—2010/324. Fort Collins, Colorado.

Renfro, A. A., J. K. Cochran, D. J. Hirschberg, H. J. Bokuniewicz, and S. L. Goodbred Jr (2016), The sediment budget of an urban coastal lagoon (Jamaica Bay, NY) determined using 234Th and 210Pb, Estuarine, Coastal Shelf Science, 180, 136–149.

Ruhl, C. A., and M. R. Simpson (2005), Computation of discharge using the index-velocity method in tidally affected areas, US Department of the Interior, US Geological Survey.

Sanderson, E.W. 2016. Cartographic evidence for historical geomorphological change and wetland formation in Jamaica Bay, New York. *Northeastern Naturalist* 23 (2): 277–304.

Shchepetkin, A.F., and J.C. McWilliams. 2005. The regional oceanic modeling system (ROMS): a split-explicit, free-surface, topography-following-coordinate oceanic model. *Ocean Modelling* 9 (4): 347–404.

Swanson, R.L., and R.E. Wilson. 2008. Increased tidal ranges coinciding with Jamaica Bay development contribute to marsh flooding. *J. Coastal. Res.* 1565-1569.

Warner, J.C., B. Armstrong, R. He, and J.B. Zambon. 2010. Development of a coupled ocean–atmosphere–wave–sediment transport (COAWST) modeling system. *Ocean Modelling* 35 (3): 230–244.

Weston, N.B. 2014. Declining sediments and rising seas: an unfortunate convergence for tidal wetlands. *Estuaries and Coasts* 37 (1): 1–23.

Wong, K.-C., and R.E. Wilson. 1984. Observations of low-frequency variability in Great South Bay and relations to atmospheric forcing. *Journal of Physical Oceanography* 14 (12): 1893–1900.

Wright, S. A., D. J. Topping, and C. A. Williams (2010), Discriminating silt-and-clay from suspended-sand in rivers using side-looking acoustic profilers, paper presented at Joint Federal Interagency Conference 2010: Hydrology and sedimentation for a changing future: existing and emerging issues.

Zaggia, L., G. Lorenzetti, G. Manfé, G.M. Scarpa, E. Molinaroli, K.E. Parnell, J.P. Rapaglia, M. Gionta, and T. Soomere. 2017. Fast shoreline erosion induced by ship wakes in a coastal lagoon: field evidence and remote sensing analysis. *PLoS One* 12 (10): e0187210.